



HAL
open science

Influence of Some Rheological Parameters On Flexure of the Oceanic Lithosphere

Andrei A Panteleyev, Michel Diament

► **To cite this version:**

Andrei A Panteleyev, Michel Diament. Influence of Some Rheological Parameters On Flexure of the Oceanic Lithosphere. *Geophysical Journal International*, 1992, 114, pp.209-220. 10.1111/j.1365-246X.1993.tb01480.x . insu-01356027

HAL Id: insu-01356027

<https://insu.hal.science/insu-01356027v1>

Submitted on 24 Aug 2016

HAL is a multi-disciplinary open access archive for the deposit and dissemination of scientific research documents, whether they are published or not. The documents may come from teaching and research institutions in France or abroad, or from public or private research centers.

L'archive ouverte pluridisciplinaire **HAL**, est destinée au dépôt et à la diffusion de documents scientifiques de niveau recherche, publiés ou non, émanant des établissements d'enseignement et de recherche français ou étrangers, des laboratoires publics ou privés.

Influence of some rheological parameters on flexure of the oceanic lithosphere

A. N. Panteleyev^{1,*} and M. Diament²

¹ Institute of Physics of the Earth, 10 B. Gruzinskaya, D-242 Moscow, Russia

² Institut de Physique du Globe de Paris, Laboratoire Gravimétrie et Géodynamique, Case 89, 4 Place Jussieu, F-75252 Paris 05, France

Accepted 1992 December 21. Received 1992 December 21; in original form 1991 December 30

SUMMARY

Rheological parameters describe properties of the lithosphere, but it is generally impossible to measure them *in situ*. Thus a model has to be developed to relate parameters to observables. We consider flexure of the oceanic lithosphere. A quantitative representation of a brittle-elastic-ductile rheology is based on a semi-empirical model. The non-linear problem of plate flexure is solved by the multiple-shooting algorithm using a Runge–Kutta procedure from analytical solutions for an elastic model. The bending moment and its derivatives have been deduced analytically to improve the accuracy and speed of computations. A family of numerical solutions was built that describes flexure of the oceanic lithosphere at subduction zones for various ages, strain rates, and activation energies. Relative contributions of rheological parameters are discussed. The model is then used to evaluate rheological parameters of the Kuril trench from gravity data. The strain rate estimates are found to be about $3 \cdot 10^{-(16 \pm 1)} \text{ s}^{-1}$ assuming creep activation energies between 520 kJ/mole and 550 kJ/mole for lithospheric age ranging from 90 Ma to 110 Ma.

Key words: flexure, gravity, oceanic lithosphere, rheology.

INTRODUCTION

Various observable features in the ocean, such as outer rises on the oceanic sides of deep-sea trenches or moats flanking seamount chains, are explained by flexure of the oceanic lithosphere (Vening–Meinesz 1941; Gunn 1943). Many studies showed that flexure of the lithosphere depends on whether the lithosphere is elastic (e.g. Vening–Meinesz 1941; Gunn 1943; Hanks 1971; Watts & Talwani 1974; Parsons & Molnar 1976; Caldwell *et al.* 1976), viscous (De Bremaecker 1977), viscoelastic (Melosh 1978), perfectly plastic (Lobkovsky & Sorokhtin 1976), or elastoplastic (McAdoo, Caldwell & Turcotte 1978; Turcotte, McAdoo & Caldwell 1978; Bodine & Watts 1979; Chapple & Forsyth 1979). Thus rheological parameters describe mechanical properties of the lithosphere (Kirby 1977; Goetze & Evans 1979; Brace & Kohlstedt 1980; Kirby 1983; Kirby & Kronenberg 1987; Ranalli & Murphy 1987). In fact, rheology controls stress and deformation of the lithosphere subjected to external forces, such as loads, as well as the evolution of deformations with time.

* Presently at Institut de Physique du Globe de Paris, Laboratoire Gravimétrie et Géodynamique, Case 89, 4 Place Jussieu, F-75252 Paris 05, France.

On the basis of the realistic brittle-elastic-ductile rock rheology of the oceanic lithosphere, Goetze & Evans (1979) suggested a multiple-layer model represented in terms of the yield stress envelope (YSE). The model was used by many authors (e.g. Bodine, Steckler & Watts 1981; McNutt & Menard 1982; McAdoo, Martin & Poulouse 1985; Chamot-Rooke & Le Pichon 1989). This model appears to explain successfully flexure observations as well as to overcome limitations of the purely elastic model (Deplus 1987) that fails to predict steep bathymetry slopes for many trenches (Caldwell *et al.* 1976) and generally requires stress in rocks which is too high based on experimental data on rock mechanics.

According to the model, in particular, flexure of the lithosphere is controlled by creep laws that act in the ductile part of the lithosphere and involve strain rate, physical state (temperature) and properties (creep-activation energy) of the rock. The thermal structure of the oceanic lithosphere has been widely discussed (e.g. Turcotte & Oxburgh 1967; Parker & Oldenburg 1973; Parsons & Sclater 1977; Cazenave 1984; Denlinger 1992; Stein & Stein 1992) and seems rather well evaluated. Creep activation energy is known from laboratory experiments (Goetze & Evans 1979). Finally, difficulty in measuring *in situ* does not permit

us to obtain directly present values of strain rate, but several authors have estimated them (Goetze & Evans 1979; Chapple & Forsyth 1979; Bodine *et al.* 1981; McNutt & Menard 1982).

Nevertheless, no complete analysis of the trade-offs between these parameters has been carried out previously. Our goal in the paper is to develop a numerical method to compute flexure of the oceanic lithosphere in order to better address this question and to investigate if *in situ* estimations of these parameters could be obtained by studying flexure.

RHEOLOGY MODEL

To treat the brittle-elastic-ductile rheology, we reduce it to the multiple-layer elastoplastic model described by means of YSE (e.g. Goetze & Evans 1979; McNutt & Menard 1982; McAdoo *et al.* 1985). Corresponding values of the highest permissible difference of the principle stresses, $\Delta\sigma_{\max} \equiv (\sigma_1 - \sigma_3)_{\max}$ or rather its signed modification $\Delta\sigma_r$ as determined by semi-empirical laws, are assigned to each lithospheric level for both compression and tension.

Upper layers of the oceanic lithosphere are exposed to brittle failure and to frictional sliding on fault surfaces. The process is controlled by Byerlee's laws (Byerlee 1978) (following Byerlee, we treat compressive stress as positive):

$$\tau = 0.85 \sigma_n \quad \text{at } \sigma_n \leq 0.2 \text{ GPa} \quad (1a)$$

$$\tau = 0.6\sigma_n + 0.05 \text{ GPa} \quad \text{at } 0.2 \text{ GPa} < \sigma_n < 2 \text{ GPa} \quad (1b)$$

where σ_n is the normal (confining) stress, and τ is the highest permissible tangent (breaking) stress. Using Mohr's circle diagram it is possible to show that the result is nearly a linear dependence of $\Delta\sigma_r$ on depth (see Appendix A for details).

Following McAdoo *et al.* (1985), we describe $\Delta\sigma_r$ in the upper oceanic lithosphere by means of two vertical gradients only: $\gamma_{\text{BC}} = 0.66 \cdot 10^5 \text{ Pa m}^{-1}$ for compression and $\gamma_{\text{BT}} = -0.22 \cdot 10^5 \text{ Pa m}^{-1}$ for tension. This approach does not take into account explicitly the sea-water loading and gives absolute values of $\Delta\sigma_r$ somewhat smaller than those from more accurate formulae derived in Appendix A. However, both descriptions seem to be more or less adequate, since water *can* penetrate into the upper layers of the oceanic lithosphere. The possible resulting serpentinization and filling of pores by fluids may then substantially decrease the strength of rocks (Kirby & Kronenberg 1987).

In general, rheology of the upper oceanic lithosphere is defined by lithostatic pressure only. It depends on the depth and, to some extent, on the specific vertical density distribution.

Lower layers of the oceanic lithosphere obey the power-creep law (2b) and its modification at higher differences of the principle stresses in Peierl's region (2a) (Goetze & Evans 1979):

$$\dot{\epsilon} = C_1 \exp \left[-\frac{Q_1}{RT} \left(1 - \frac{\sigma_1 - \sigma_3}{\sigma_0} \right)^2 \right], \quad \text{at } \sigma_1 - \sigma_3 > 0.2 \text{ GPa} \quad (2a)$$

$$\dot{\epsilon} = C_2 (\sigma_1 - \sigma_3)^n \exp \left(-\frac{Q_2}{RT} \right), \quad n = 3, \quad \text{at } \sigma_1 - \sigma_3 \leq 0.2 \text{ GPa} \quad (2b)$$

where T is absolute temperature in K , $\dot{\epsilon}$ is strain rate in s^{-1} , $R = 8.314 \text{ J/(K} \cdot \text{mole)}$, $C_1 = 5.7 \cdot 10^{11} \text{ s}^{-1}$, $C_2 = 7.0 \cdot 10^{-14} \text{ s}^{-1} \text{ Pa}^{-3}$, $\sigma_0 = 8.5 \text{ GPa}$; $Q_1 = 536 \text{ kJ/mole}$ and $Q_2 = 523 \text{ kJ/mole}$ are respective activation energies. σ_1 and σ_3 are the maximal and the minimal principle stresses respectively so that always $\sigma_1 - \sigma_3 \geq 0$. Unlike Byerlee's laws (1), there is no dependence on σ_n . As a result, relative to compression and tension the laws (2) are symmetrical.

The relations (2) are obtained from experimental studies of dunites containing dry olivine that represent the upper mantle rocks. According to (2), the relationship between $\dot{\epsilon}$ and $\sigma_1 - \sigma_3$ strongly depends on temperature, hence on depth below the surface of the plate and on the lithospheric age.

The temperature distribution with depth is computed using cooling models of the oceanic lithosphere. Since recent studies note opposing effects that can place standard isotherms both shallower (Stein & Stein 1992) and deeper (Denlinger 1992) than generally accepted cooling models predict, we adopt, following McAdoo *et al.* (1985), the simple half-space model (Turcotte & Oxburgh 1967; Parker & Oldenburg 1973) for ages 80 Ma or less:

$$T = T_0 \text{ erf} \{z/[2(kt)^{1/2}]\}, \quad t \leq 80 \text{ Ma} \quad (3a)$$

and for ages greater than 80 Ma we use the following first-order approximation of the plate model (Parsons & Sclater 1977):

$$T \equiv T_0 \left[\frac{z}{a} + \frac{2}{\pi} \sin \left(\frac{\pi z}{a} \right) \exp \left(-\frac{\pi^2 kt}{a^2} \right) \right], \quad t > 80 \text{ Ma} \quad (3b)$$

where T is temperature, $^\circ\text{C}$, T_0 is zero-age temperature, k is thermal diffusivity, t is age, z is depth, a is thermal plate thickness. We use $T_0 = 1300 \text{ }^\circ\text{C}$, $a = 125 \text{ km}$, and $k = 10^{-6} \text{ m}^2 \text{ s}^{-1}$.

We deal with lithospheres older than 30 Ma, so we do not need to distinguish the young lithosphere cooling regime (Cazenave 1984) as well as formation processes of the lithosphere in the vicinity of mid-ocean ridges. We perform computations to an age of 160 Ma.

To constrain YSE, we fix different strain-rate distributions with depth in the lower oceanic lithosphere (e.g. Goetze & Evans 1979; Bodine *et al.* 1981; McNutt & Menard 1982; McAdoo *et al.* 1985; Chamot-Rooke & Le Pichon 1989). Each distribution is considered to be the limit of the elastic stress and the border between elastic and plastic regimes, such that the strain rate and the temperature of a layer are unequivocally associated with $\Delta\sigma_r$. We varied the strain rate from 10^{-19} s^{-1} to 10^{-13} s^{-1} ; assuming that strains of a few per cent develop over 10^7 yr , a simple kinematic scheme (e.g. Goetze & Evans 1979) gives $\dot{\epsilon} = 10^{-15} \text{ s}^{-1}$, whilst more elaborate estimates provide strain rate from 10^{-18} s^{-1} or 10^{-17} s^{-1} under seamounts and up to 10^{-16} s^{-1} or 10^{-15} s^{-1} at subduction zones (Bodine *et al.* 1981; McNutt & Menard 1982). Other authors (e.g. Chamot-Rooke & Le Pichon 1989, and McAdoo *et al.* 1985, for the lower oceanic lithosphere; Fadaie & Ranalli 1990, for the continental one) usually assume strain rate to be of the order of 10^{-16} s^{-1} or 10^{-15} s^{-1} to model rheology.

A change in the strain rate by an order of magnitude makes a noticeable effect on YSE that is larger than the error introduced by the approximation of YSE (see Fig. 1). The depth where the linearized $\Delta\sigma_r$ equals zero is

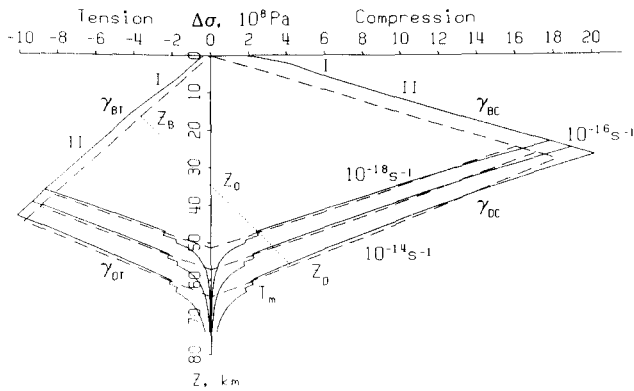


Figure 1. YSE for the oceanic lithosphere, i.e. $\Delta\sigma_r$ (see text and Appendices), 10^8 Pa, horizontal axis, versus depth from the top of the lithosphere, km, vertical axis. Curves are shown for 90 Ma old lithosphere. Byerlee's laws I(1a) and II(1b) are shown for the upper lithosphere as deduced in Appendix A, eq. (A12), in as much as the linear approximation after McAadoo *et al.* (1985) was used for computation (dashed lines). Three values of the lower lithosphere strain rate are shown: 10^{-18} s^{-1} , 10^{-16} s^{-1} , 10^{-14} s^{-1} . The linearized $\Delta\sigma_r$ are also shown with dashes. Differences of the principle stresses $\Delta\sigma_r$ in the intermediate elastic layer are shown by dotted line. T_m denotes the thickness of the mechanical lithosphere, z_B and z_D designate the upper and the lower depth borders of the elastic layer, z_0 shows the neutral plane that does not coincide generally with the middle plane of the plate due to the asymmetry of YSE. The vertical gradients of $\Delta\sigma_r$ are denoted by γ_{BC} (brittle compression), γ_{DT} (ductile tension), γ_{BT} (brittle tension), and γ_{DC} (ductile compression).

considered to be the base of the mechanical oceanic lithosphere, z_b . The thickness of the lithosphere above this level corresponds to the thickness of the mechanical lithosphere, T_m . As a result the lower part of YSE can be described by means of two values: T_m and the absolute value of the vertical gradients of $\Delta\sigma_r$, $\gamma_L = |\gamma_{DT}| = |\gamma_{DC}|$. Since

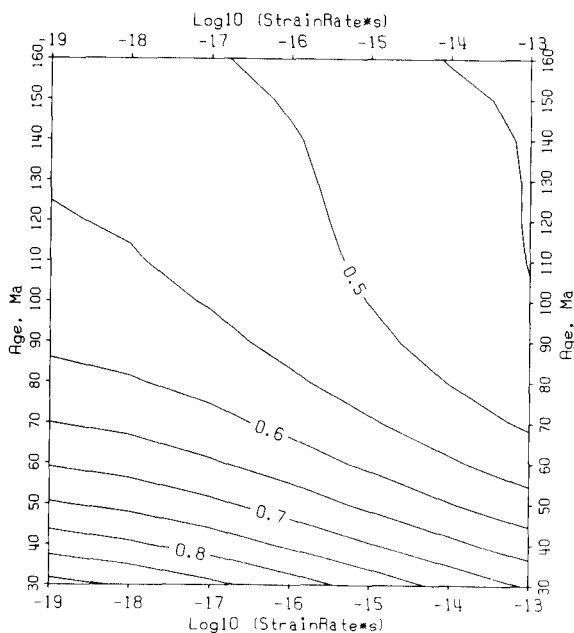


Figure 2. Absolute value of the vertical gradients of $\Delta\sigma_r$ in the lower ductile part of the oceanic lithosphere, γ_L , 10^5 Pa m^{-1} , as a function of the strain rate $\dot{\epsilon}$: $\log_{10}[\dot{\epsilon}(\text{s}^{-1}) \cdot \text{s}]$, horizontal axis, and the lithospheric age, Ma, vertical axis.

the upper part of YSE has a constant description, T_m and γ_L are the only variable parameters of the model.

The 2-D distributions of values of T_m and γ_L with the lithospheric age and with the strain rate were computed. Figs 2 and 3(a) show that (and how) ancient oceanic lithosphere subjected to slow deformations (low strain rate) at its base has the same strength properties as the younger oceanic lithosphere subjected to faster deformations. This tendency was previously noted by Bodine *et al.* (1981).

Our computations show that the temperature at the base of the plate (depth z_b) depends on strain rate at a given activation energy (Table 1): if the strain rate is higher, then warmer zones of the lithosphere are included in T_m . It

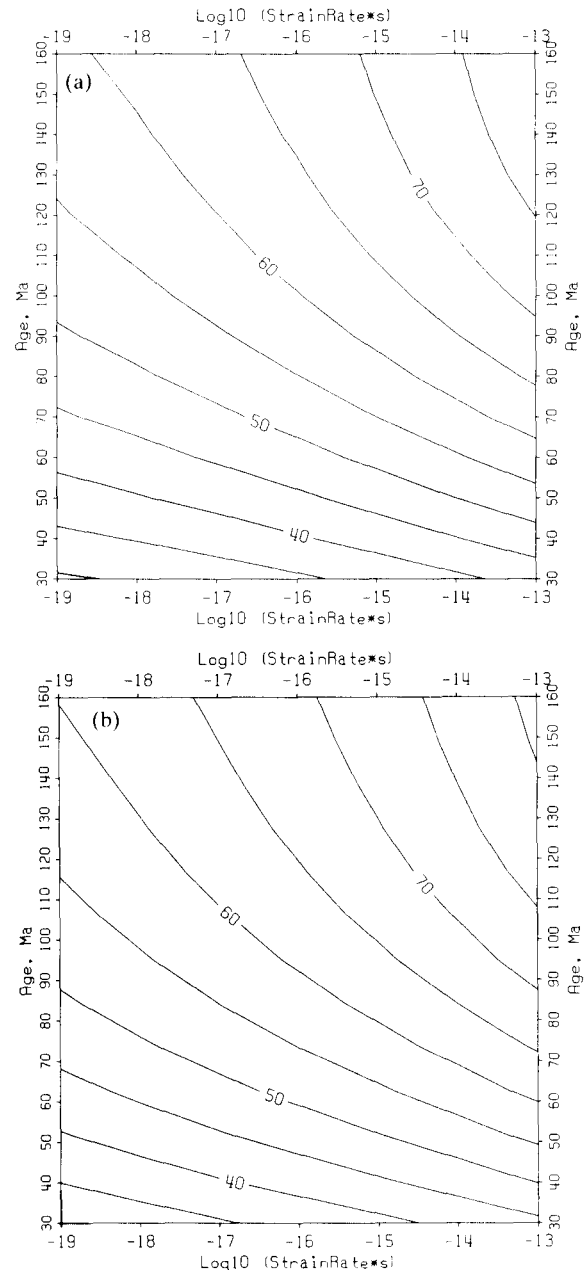


Figure 3. T_m (see text), km, as a function of the strain rate $\dot{\epsilon}$: $\log_{10}[\dot{\epsilon}(\text{s}^{-1}) \cdot \text{s}]$, horizontal axis, and the lithospheric age, Ma, vertical axis. Two sets of activation energies are represented: (a) $Q_1 = 536 \text{ kJ/mole}$ and $Q_2 = 523 \text{ kJ/mole}$; (b) $Q_1 = Q_2 = 550 \text{ kJ/mole}$.

Table 1. Temperature at the base of the mechanical oceanic lithosphere, z_b , as the function of the strain rate (see text). Computation was done assuming activation energy values after Goetze & Evans (1979): $Q_1 = 536$ kJ/mole and $Q_2 = 523$ kJ/mole.

strain rate, s^{-1}	10^{-19}	10^{-18}	10^{-17}	10^{-16}	10^{-15}	10^{-14}	10^{-13}
Temperature, $^{\circ}C$	645 ± 4	670 ± 4	700 ± 4	735 ± 4	770 ± 5	810 ± 5	850 ± 5

follows that T_m depends on both the strain rate (that defines temperature at depth z_b) and the lithospheric age (that defines vertical temperature distribution). More accurately, there is also a slight decrease of temperature at depth z_b with age, in particular for the younger lithosphere, higher strain rates and activation energies. As a result temperatures for the lithospheric age of 30 Ma are about $10^{\circ}C$ higher than those shown in Tables 1 and 2. Results shown in Tables 1 and 2 appear to be constant for ages ranging from 50 Ma to 160 Ma. Tables 1 and 2 indicate that an increase of activation energies by an order of 4 per cent increases the temperature at depth z_b by $30 \pm 5^{\circ}C$ that conforms to an increase of T_m by 2.1 ± 0.9 km (larger increases of temperature and T_m correspond to higher strain rate; a larger increase of T_m is also associated with older ages).

We use activation energies given by Goetze & Evans (1979): $Q_1 = 536$ kJ/mole and $Q_2 = 523$ kJ/mole. An increase of them by roughly 4 per cent for young, slowly deforming lithosphere or up to 10 per cent for the old, rapidly deforming lithosphere is nearly equivalent to flexure of the lithosphere at a strain rate increased by an order of magnitude (Fig. 3). On the other hand, a 4 per cent increase of the two activation energies gives rise to changes of the flexural properties of the lithosphere that are similar to those arising when the lithosphere grows old by approximately one eighth of its age (Fig. 3).

Clearly strain rate, creep-activation energies, and thermal structure of the lithosphere together affect mechanical properties of the lithosphere so that it is very difficult to separate their contributions. However, they may be estimated from studying flexure of the lithosphere in view of additional considerations.

MECHANICAL MODEL

Flexure of the oceanic lithosphere can be studied beneath seamounts or in the vicinity of subduction zones. We chose to model the subducting lithosphere in order to avoid complexities arising from poor knowledge of shape of weak flexure, peripheral basin infilling, and deep heterogeneities, as well as from rejuvenation of the lithosphere at hot spots.

The subducting oceanic lithosphere is taken as a thin plate overlain by sea water and underlain by heavy liquid as dense as upper mantle rocks (Fig. 4). Assuming no horizontal external forces which might be important only for very thin lithosphere (e.g. Turcotte & Schubert 1982), the equation of equilibrium is

$$\frac{d^2M}{dx^2} + (\rho_m - \rho_w)gw = 0 \quad (4)$$

Table 2. Same as Table 1 but with larger activation-energy values: $Q_1 = Q_2 = 550$ kJ/mole.

strain rate, s^{-1}	10^{-19}	10^{-18}	10^{-17}	10^{-16}	10^{-15}	10^{-14}	10^{-13}
Temperature, $^{\circ}C$	670 ± 3	700 ± 4	730 ± 4	765 ± 5	800 ± 5	840 ± 5	885 ± 5

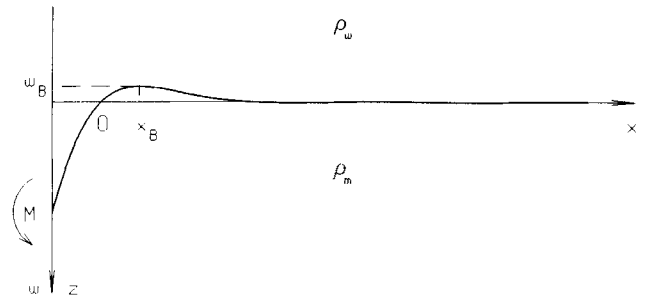


Figure 4. Mechanical model of the subducting plate:

bending moment M —positive counterclockwise; z -axis, deflection w —positive downward, w_B —the outer-rise height; x -axis—positive oceanward, $w(x_B) = w_B$; sea-water density $\rho_w <$ mantle-rock density ρ_m . We select the coordinate-axes start point so that $w|_{x=0} = 0$. It is treated as the 'zero point': at the trench axis $x < 0$, at the outer rise $x > 0$.

where M is the flexural moment (counterclockwise positive), x is horizontal coordinate, positive oceanward, ρ_m and ρ_w are densities of the upper mantle rock and of the sea water (we later used $\rho_m - \rho_w = 2.30 \cdot 10^3$ kg m^{-3}), $g = 9.8$ m s^{-2} is gravity acceleration, and w is vertical deflection of the plate. Eq. (4) is valid for any kind of rheology. In our case we deduce the non-linear ordinary differential equation in the complete form.

We do not allow any total compressive or tensile force along the plate, so we define 'the bending stress' as $\Delta\sigma(x, z) = \sigma_{xx}(x, z) - \sigma_{zz}(x, z)$. It is well known for the elastic layer (Turcotte & Schubert 1982) that

$$\Delta\sigma(x, z) = \frac{(z - z_0)E d^2w(x)}{1 - \nu^2 dx^2} \quad (5)$$

where z is depth counted down from the top of the lithosphere, z_0 is depth to the neutral plane, E is Young's modulus, and ν is Poisson's ratio. In the elastic layer we set $E = 7 \cdot 10^{10}$ Pa and $\nu = 0.25$. From (5), the bending moment for the purely elastic layer is

$$M(x) = D \frac{d^2w(x)}{dx^2} \quad \text{with} \quad D \equiv \frac{ET_e^2}{12(1 - \nu^2)} \quad (6)$$

where D is rigidity, and T_e is thickness of the elastic layer. Substitution of (6) in (4) gives a linear differential equation. Its solution is

$$w(x) = e^{-x/\lambda} [C_1 \cos(x/\lambda) + C_2 \sin(x/\lambda)] + e^{x/\lambda} [C_3 \cos(x/\lambda) + C_4 \sin(x/\lambda)] \quad (7)$$

where $\lambda = [4D(\rho_m - \rho_w)^{-1} g^{-1}]^{1/4}$ is the flexural parameter; C_1, C_2, C_3, C_4 are constants defined from boundary conditions, as a rule $C_3 = C_4 = 0$ to prevent any exponential growth of the solution (7) at $x \rightarrow \infty$. By selecting the starting point of the horizontal coordinate, another constant is excluded, for instance, $w(x) = C_2 e^{-x/\lambda} \sin(x/\lambda)$.

The vertical gradient of stress in the elastic layer as derived from (5) is

$$\gamma(x) = \frac{\partial \Delta\sigma(x, z)}{\partial z} = \frac{E}{1 - \nu^2} \frac{d^2w(x)}{dx^2} \quad (8)$$

The eq. (4) is written assuming that thickness of the plate is negligible as compared to the flexure radius. Thus we have a

physical restriction for (8) in our approach:

$$|\gamma| = \frac{E}{1-\nu^2} \left| \frac{d^2 w(x)}{dx^2} \right| \ll \frac{7 \cdot 10^{10} \text{ Pa}}{1-0.25^2} \cdot 10^{-5} \text{ m}^{-1} \\ \approx 0.8 \text{ MPa m}^{-1}.$$

It is also possible to show that this restriction prohibits considering cases in which the intermediate elastic layer between the brittle and ductile zones somewhere is less than about 3 km.

In addition we assume also that the upper and lower bounds of the intermediate elastic layer lie respectively in the brittle and ductile portions of the YSE. If the plate is convex upward, the last condition is always satisfied due to $|\gamma_{BC}| > |\gamma_{BT}|$ and $\gamma_{DC} = -\gamma_{DT} < \gamma_{BT} < 0$ (see Appendices and results of computations of γ_L in Fig. 2). If the plate is convex downward, it is possible to show that the condition may be violated only by very strong flexure of the plate edge upward: it requires a 5 km elevation of the relief in a 100 km horizontal distance due to the downward-convex plate flexure only. Such flexure does not seem to occur in nature.

Using notations T_m , z_B , z_D , and z_0 of Fig. 1, and assuming zero horizontal external force, we get

$$z_B = \frac{\gamma z_0}{\gamma - \gamma_B} \quad \text{and} \quad z_D = \frac{\gamma z_0 - \gamma_D T_m}{\gamma - \gamma_D}$$

that allows us to deduce

$$\int_0^{T_m} \Delta\sigma(x, z) dz = \int_0^{z_B(\gamma)} z \gamma_B dz + \int_{z_B(\gamma)}^{z_D(\gamma)} (z - z_0) \gamma dz \\ + \int_{z_D(\gamma)}^{T_m} (z - T_m) \gamma_D dz \\ = \frac{\gamma}{2} \cdot \left[\frac{\gamma_D}{\gamma_D - \gamma} (T_m - z_0)^2 - \frac{\gamma_B}{\gamma_B - \gamma} z_0^2 \right] = 0 \quad (9)$$

where γ_B and γ_D denote either γ_{BC} and γ_{DT} , or γ_{BT} and γ_{DC} . We consider γ_B and γ_D as independent from z and later also from x . This assumption for upper brittle layers of the lithosphere is a consequence of our model. As concerning lower ductile layers, γ_D depends on strain rate that changes along the plate and probably with depth. The lower ductile layers represent a relatively thin part of the lithosphere so that vertical distribution of strain rate there seems to be quasi-constant (obviously we can neglect changes substantially less than an order of magnitude of strain rate). A relative distribution of strain rate along a subducting plate perpendicular to the trench was obtained by Chapple & Forsyth (1979). In particular, a pronounced peak of strain rate was shown close to the trench. According to estimations cited above, far from the trench the strain rate is less about two or three orders of magnitude that diminishes YSE, but plate curvature, bending stresses and moment vanish much faster. In addition, far from the trench radius of plate curvature is very large so that it is comparable with the radius of the earth and we cannot consider so fine effects in our plane 2-D model. Thus in our approach it seems to be natural to treat YSE as constant.

From (9) we have immediately

$$z_0[\gamma(x)] = \frac{T_m}{1 + \sqrt{\frac{\gamma_B \cdot \gamma_D - \gamma}{\gamma_D \cdot \gamma_B - \gamma}}} \quad (10)$$

The bending moment takes the following form:

$$M[\gamma(x)] = \int_0^{T_m} \Delta\sigma(x, z) [z - z_0(\gamma)] dz \\ = \int_0^{z_B(\gamma)} \gamma_B z \cdot [z - z_0(\gamma)] dz \\ + \int_{z_B(\gamma)}^{z_D(\gamma)} \gamma \cdot [z - z_0(\gamma)]^2 dz \\ + \int_{z_D(\gamma)}^{T_m} \gamma_D \cdot (z - T_m) [z - z_0(\gamma)] dz \\ = \frac{\gamma^3 z_0^3(\gamma)}{6(\gamma_B - \gamma)^2} - \frac{[\gamma z_0(\gamma) - \gamma_D T_m]^3}{6(\gamma_D - \gamma)^2} - \frac{\gamma_D}{6} T_m^3. \quad (11)$$

It follows from (10) and (11) that at infinitesimal flexure

$$\lim_{\gamma \rightarrow 0} z_0(\gamma) = T_m/2, \quad \lim_{\gamma \rightarrow 0} M(\gamma) = 0,$$

and

$$\lim_{\gamma \rightarrow 0} M(\gamma)/\gamma = T_m^3/12$$

so that, as compared to (6) and (8), the plate behaves like it is purely elastic. On the other hand, for the upward convex plate (10) gives

$$\lim_{\gamma \rightarrow +\infty} z_0(\gamma) = T_m / (1 + \sqrt{\gamma_{BT}/\gamma_{DC}}),$$

$$\lim_{\gamma \rightarrow +\infty} M(\gamma) = -\gamma_{BT} T_m^3 / [6(1 + \sqrt{\gamma_{BT}/\gamma_{DC}})]$$

i.e. the permissible bending moment is substantially limited (restrictions do also exist for the downward convex one but may not be reached in fact). We note that the so-called effective rigidity was used by many authors (e.g. Bodine *et al.* 1981; McAdoo *et al.* 1985; Chamot-Rooke & Le Pichon 1989). Similar to (6) and using (8) it can be defined as $D_{\text{eff}}(\gamma) = M(\gamma)E/[(1-\nu^2)\gamma]$. Obviously it depends on γ , i.e. on x , so that its using in (4) requires to take into account also its derivatives.

We do not deal with the effective rigidity, but deduce directly derivatives of the bending moment to present eq. (4) in the complete form for our rheology. Implying that

$$\gamma' = \frac{d\gamma(x)}{dx}, \quad \text{we note:}$$

$$\frac{dz_0[\gamma(x)]}{dx} = \frac{dz_0(\gamma)}{d\gamma} \gamma' = \frac{\gamma_B \cdot (\gamma_B - \gamma_D) z_0^3 \gamma'}{2\gamma_D \cdot (\gamma_B - \gamma)^2 (T_m - z_0) T_m}$$

that gives $dM(x)/dx = \gamma' F(\gamma)$ where

$$F(\gamma) = \frac{(3\gamma_B - \gamma)\gamma^2}{6(\gamma_B - \gamma)^3} z_0^3 + \frac{(\gamma_D T_m - \gamma z_0)^2}{6(\gamma_D - \gamma)^3} \\ \times [(\gamma - 3\gamma_D)z_0 + 2\gamma_D T_m] \\ + \frac{\gamma\gamma_B \cdot (\gamma_B - \gamma_D) z_0^3}{4\gamma_D \cdot (\gamma_B - \gamma)^2 (T_m - z_0) T_m} \\ \times \left[\frac{\gamma^2 z_0^2}{(\gamma_B - \gamma)^2} - \frac{(\gamma_D T_m - \gamma z_0)^2}{(\gamma_D - \gamma)^2} \right] \quad (12)$$

with z_0 from (10). Further,

$$\frac{d^2M(x)}{dx^2} = \gamma^n F(\gamma) + \gamma'^2 F'(\gamma)$$

where

$$F'(\gamma) \equiv \frac{dF(\gamma)}{d\gamma} = \frac{\gamma\gamma_B^2 z_0^3}{(\gamma_B - \gamma)^4} + \frac{(\gamma_D T_m - \gamma z_0)\gamma_D^2}{(\gamma_D - \gamma)^4} \cdot (T_m - z_0)^2 + \frac{3\gamma^2 \gamma_B^2 \cdot (\gamma_B - \gamma_D) z_0^5}{2(\gamma_B - \gamma)^5 \gamma_D \cdot (T_m - z_0) T_m} + \frac{(\gamma_D T_m - \gamma z_0)\gamma_B \cdot (\gamma_B - \gamma_D) z_0^3}{2(\gamma_B - \gamma)^3 (\gamma_D - \gamma)^3 \gamma_D \cdot (T_m - z_0) T_m} \times [(2\gamma^2 - \gamma\gamma_B - \gamma_B \gamma_D)\gamma_D T_m - (2\gamma\gamma_D + \gamma\gamma_B - 3\gamma_B \gamma_D)\gamma z_0] + \frac{\gamma\gamma_B^2 \cdot (\gamma_B - \gamma_D)^2 z_0^5}{8(\gamma_B - \gamma)^4 \gamma_D^2 \cdot (T_m - z_0)^3 T_m^2} \times \left[\frac{5T_m - 4z_0}{(\gamma_B - \gamma)^2} \gamma^2 z_0^2 + \frac{\gamma_D T_m - \gamma z_0}{(\gamma_D - \gamma)^2} \right. \\ \left. \times (-4\gamma z_0^2 + 5\gamma z_0 T_m + 2\gamma_D z_0 T_m - 3\gamma_D T_m^2) \right]. \quad (13)$$

Finally we define another function: $\beta(x) = Ew(x)/(1 - \nu^2)$. We get by substituting (13) in (4) and keeping in mind that $\beta'' = \gamma$:

$$\beta^{(4)} = - \frac{\beta^{(3)2} F'(\beta'') + \frac{1 - \nu^2}{E} g \cdot (\rho_m - \rho_w) \beta}{F(\beta'')} \quad (14)$$

where F and F' are defined in (12) and (13). We obtain an essentially non-linear differential equation of the fourth order.

For the fourth-order eq. (14) the boundary problem requires four boundary conditions. We showed that the plate at infinitesimal flexure appears to be purely elastic. It

is obvious that the solution must be bounded at $x \rightarrow \infty$, but there is no general solution in the complete form for the non-linear eq. (14) to put $C_3 = C_4 = 0$ similar to (7). Nevertheless we can represent the same conditions in a different form. By differentiating (7) for three times we obtain a system of four linear equations. It is easy to show that $C_3 = C_4 = 0$ is equivalent to

$$\begin{cases} w(x) + \lambda \frac{dw(x)}{dx} + \frac{\lambda^2 d^2w(x)}{2 dx^2} = 0 \\ \frac{dw(x)}{dx} + \lambda \frac{d^2w(x)}{dx^2} + \frac{\lambda^2 d^3w(x)}{2 dx^3} = 0 \end{cases} \quad (15)$$

taken at any point of the purely elastic plate. For our plate these conditions should be assigned to some far point such that $x/\lambda \gg 1$ where λ may be defined analogous to (7). The position of the point is to be controlled during the numerical solution so that results of computations would remain stable.

Two other conditions can be assigned from measurements near the trench:

$$\begin{cases} w(x_i) = w_i \\ w'(x_i) = w'_i \end{cases} \quad (16)$$

For instance, at the crest of the outer rise w_i equals its height w_B (Fig. 4), and $w'_i = 0$.

It is easy to see that eq. (4) in form (14) can be solved by the Runge-Kutta procedure. We used such fourth-order procedure within the framework of a multiple-shooting algorithm. The shooting was realized from the purely elastic solution derived analytically to the solution of the non-linear problem by step-by-step increase in the non-linearity of the problem.

RESULTS OF MODELLING

A family of numerical solutions has been built that describes the flexure of the oceanic lithosphere at subduction zones. Fig. 5 shows an example from the family. The oceanic part behaves purely elastically since it is not flexed and $\Delta\sigma_r$ is not reached. Substantial changes in thickness of brittle, ductile

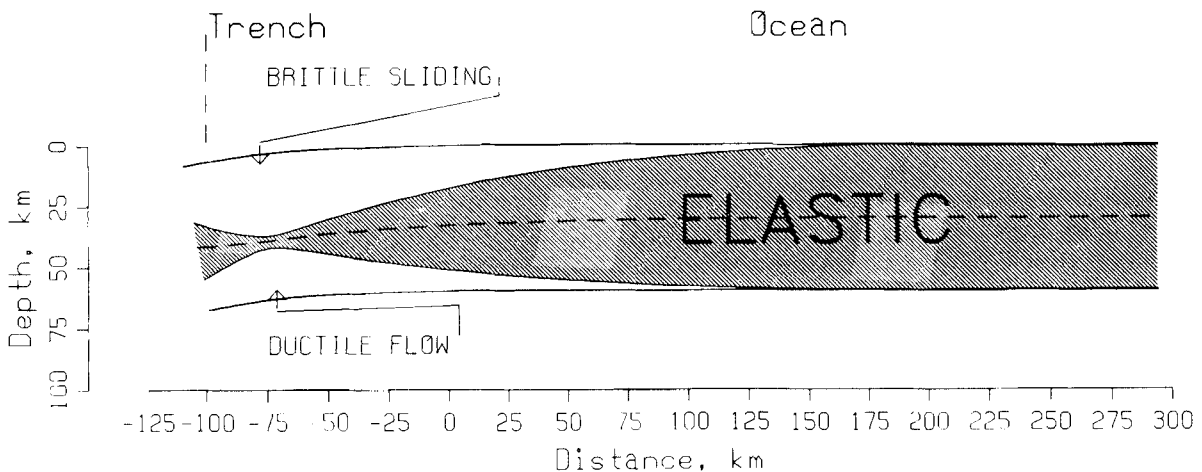


Figure 5. A computed structure of a 100 Ma old oceanic lithosphere exposed to the lower-lithosphere strain rate of 10^{-16} s^{-1} , which means $T_m = 60 \text{ km}$ (an example from the family of solutions, see text). An outer rise crest as high as $w_B = 423 \text{ m}$ is located at a distance of $x_B = 84 \text{ km}$ to the right from the 'zero point' (see Fig. 4). The most intense flexure (corresponding to the minimal thickness of the intermediate elastic layer) is obtained at a distance of $|x_H| = 74 \text{ km}$ to the left from the 'zero point'. A dashed line inside of the elastic layer shows the neutral plane.

and intermediate elastic layers are observed. The intermediate elastic layer has a pronounced thickness minimum. As is well known (e.g. Watts & Talwani 1974) the flexure induced by the subduction results in an outer rise bulge. It is too small to be observed in Fig. 5 simply because of the uniform vertical and horizontal scales.

Figure 6 shows that for a given set of activation energies, age and strain rate, our model can produce various outer-rise heights and oceanic slopes in the trench while the bulge length remains nearly constant. One would think slope observations in addition to outer rise height data are necessary to deduce T_m . Nevertheless, it would be useful only for a relatively weak flexure, for instance, at seamounts. Oceanic slopes in trenches are steep so that strong flexure may only give rise to them. 'Strong flexure' means that the bending moment is close to being saturated, the intermediate elastic layer is almost degenerated and the outer-rise height reaches its maximum. In fact the outer rise height of 90 per cent of its maximum makes the slope as steep as 4° only. On the other hand, a 1 m increase of the outer rise crest at strong flexure makes the intermediate elastic layer 0.4 km thinner with sharp steepening of the slope. Thus the lithosphere flexure model for subduction zones should imply outer-rise heights not less than about 99 per cent of their maximal allowed values.

The computations have shown that (and how) the height (Fig. 7) and the location (Fig. 8) of the outer-rise crest, the respective free-air gravity anomaly (Fig. 9) as well as the location of the most intense flexure of the oceanic lithosphere (Figs 10 and 11) depend on the lithospheric age and the lithosphere strain rate, and hence on activation energies in the manner discussed above. We note that the most intense flexure area whose location is prescribed by Figs 10 and 11 should contain extremely high vertical gradient of difference of the principle stresses so that it may be very active seismically.

A gravity effect of a flexed lithospheric plate was computed by Parker's algorithm (Parker 1972) which is very

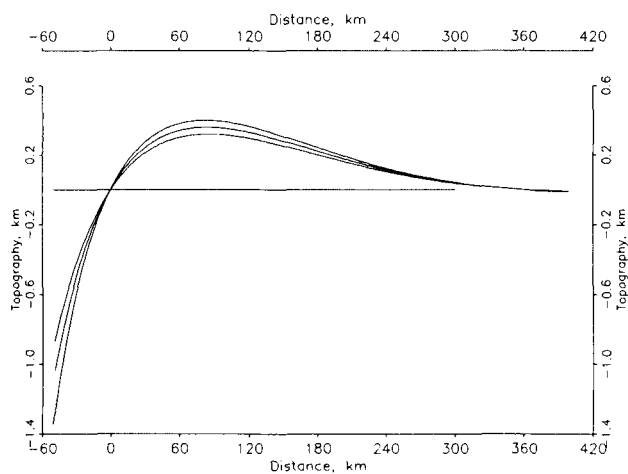


Figure 6. Outer-rise topography of 90 Ma old lithosphere exposed to the lower-lithosphere strain rate of 10^{-16} s^{-1} , which means $T_m = 57 \text{ km}$. Solutions for the outer-rise crest heights $|w_B|$ of 400 m, 360 m, and 320 m (99 per cent, 89 per cent and 79 per cent of the maximal permissible height respectively) are shown. Coordinate axes correspond to Figs 4 and 5. The vertical scale is 150 times greater than the horizontal one. The zero level is shown.

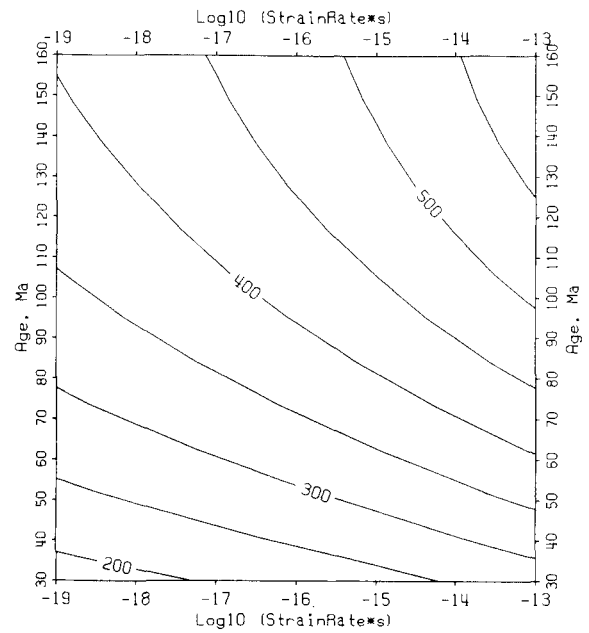


Figure 7. Maximal allowed outer-rise height $|w_B|$, m, as a function of the strain rate $\dot{\epsilon}$: $\log_{10}[\dot{\epsilon}(\text{s}^{-1}) \cdot \text{s}]$, horizontal axis, and the lithospheric age, Ma, vertical axis.

fast. Unlike geoid, free-air gravity anomalies are almost insensitive to the way of modelling of the continental slope of the trench. At the same time this algorithm is stable even if steep slopes in trenches are present. In such cases it is sufficient to take into account additional terms of expansion (usually up to 8). The number of terms was determined by comparison with the method of Talwani, Worzel & Landisman (1959). Computations were made for an oceanic lithosphere composed of three layers (crust sedimentary rocks and basalts, then upper mantle rocks) of different

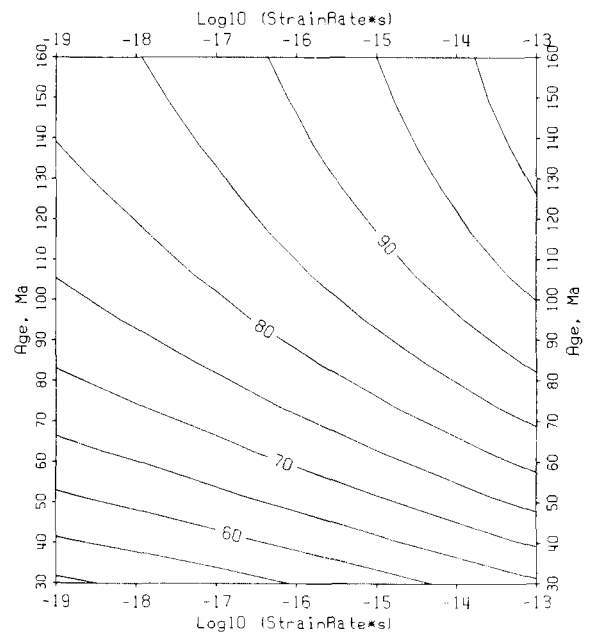


Figure 8. Outer-rise crest location (to the right from the 'zero point', see Fig. 4) x_B , km, as a function of the strain rate $\dot{\epsilon}$: $\log_{10}[\dot{\epsilon}(\text{s}^{-1}) \cdot \text{s}]$, horizontal axis, and the lithospheric age, Ma, vertical axis.

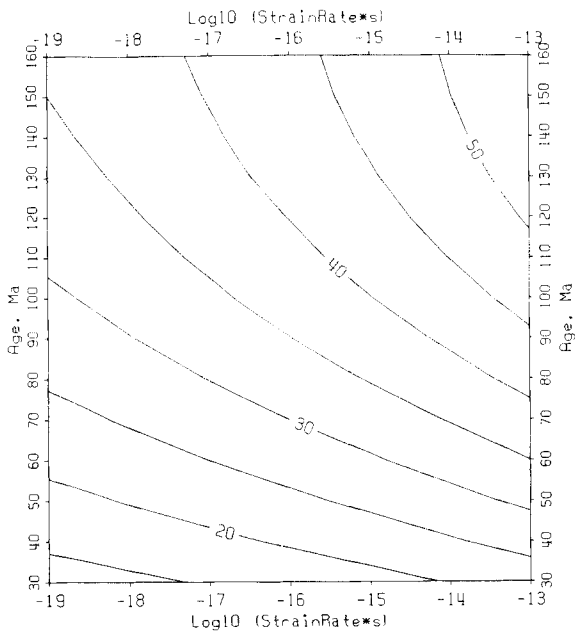


Figure 9. Maximal free-air gravity anomaly over the outer-rise Δg_B , mGal, as a function of the lithospheric age, Ma, vertical axis, and the strain rate $\dot{\epsilon}: \log_{10} [\dot{\epsilon}(\text{s}^{-1}) \cdot \text{s}]$, horizontal axis.

densities. We assume density contrasts to be 1500 kg m^{-3} (sea water—crust sedimentary rocks) at the depth of 5 km beneath the ocean surface, 300 kg m^{-3} (sedimentary rocks—basalts) at the depth of 1 km beneath the ocean floor, and 500 kg m^{-3} (crust—mantle) at the depth of 7 km beneath the ocean floor.

Figures 7–11 also show that flexure of the young lithosphere, less than about 70 Ma, is mainly controlled by the age, while for the flexure of the older lithosphere, more than 100 Ma particularly, the strain rate is more significant. This result for an ancient lithosphere is illustrated in Fig. 12.

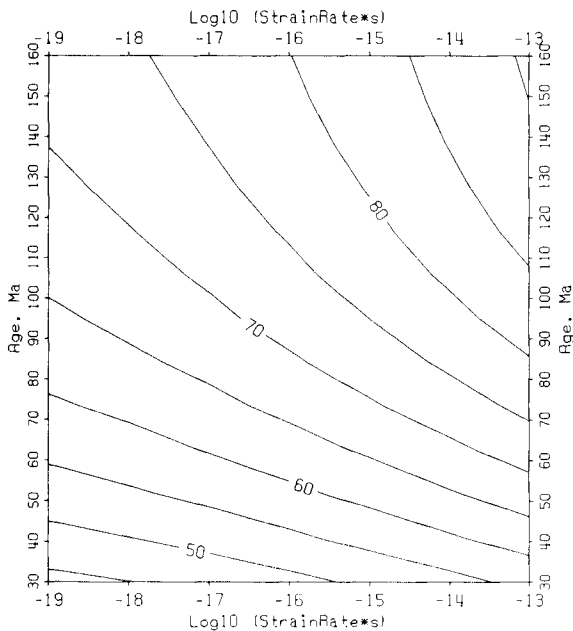


Figure 10. Location of the most intense flexure of the oceanic lithosphere (to the left from the 'zero point', see Fig. 4) x_{H1} , km, as a function of the strain rate $\dot{\epsilon}: \log_{10} [\dot{\epsilon}(\text{s}^{-1}) \cdot \text{s}]$, horizontal axis, and the lithospheric age, Ma, vertical axis.

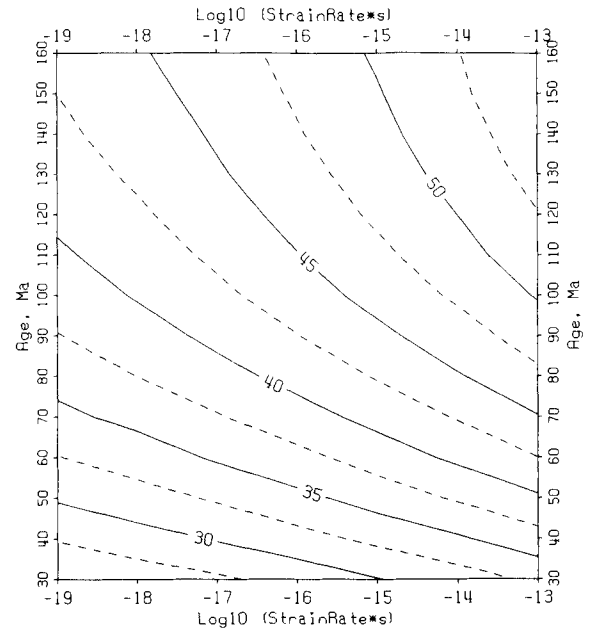


Figure 11. Domain depth beneath the sea-surface z_{H1} , km, of the minimal thickness of the intermediate elastic layer (at the most intense flexure area) as a function of the lithospheric age, Ma, vertical axis, and the strain rate $\dot{\epsilon}: \log_{10} [\dot{\epsilon}(\text{s}^{-1}) \cdot \text{s}]$, horizontal axis.

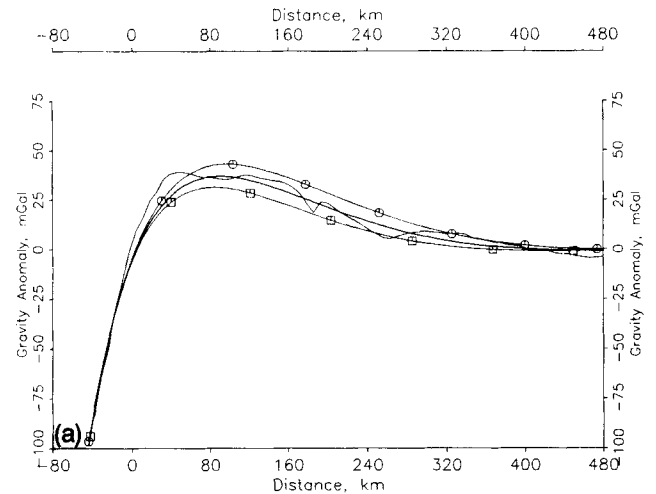


Figure 12. Superposed free-air gravity-anomaly profiles. Broken curve: interpolated shipboard data across the Kuril trench (100 Ma old lithosphere) along an orthodromic line from the point 45°N , 151°E by the initial azimuth 142° .

Middle line: a model profile (lithospheric age 100 Ma, strain rate 10^{-16} s^{-1} , hence $T_m = 60 \text{ km}$) selected by minimization of rms deflections from the shipboard data profile.

Two pairs of model profiles are shown (thin lines) to demonstrate the influence of the strain rate and age variations:

- (a) (the lower line) lithospheric age 100 Ma, strain rates 10^{-18} s^{-1} and 10^{-14} s^{-1} (the upper line);
- (b) (the lower line) strain rate 10^{-16} s^{-1} , lithospheric age 90 Ma and 110 Ma (the upper line).

The horizontal coordinate axes correspond to Figs 4 and 5.

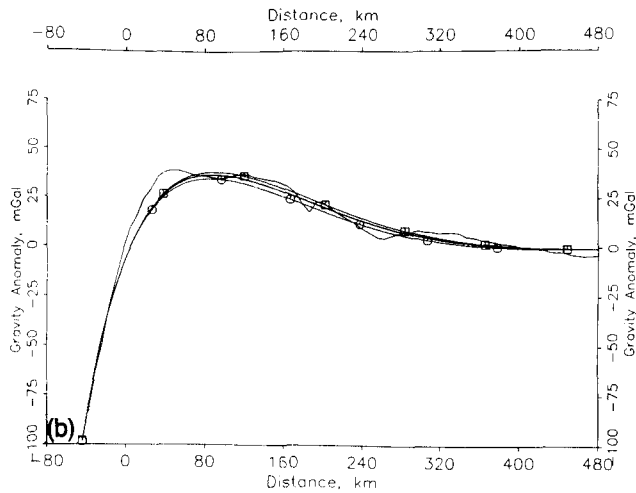


Figure 12. (Continued.)

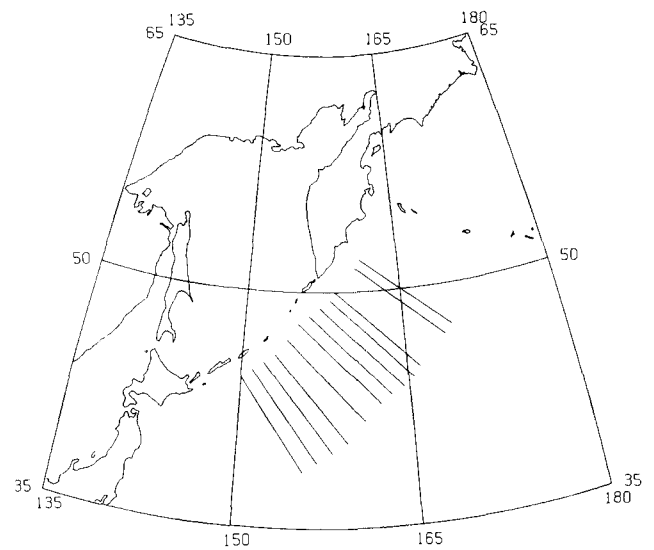


Figure 13. The Kuril trench area. North latitude and east longitude in degrees are noted on the border of the coordinate grid. The location of selected data profiles is shown.

Therefore, if the age of an ancient subducting lithosphere is reasonably well known, i.e. with an accuracy of about 10 Ma, the modelling of flexure allows estimation of the *in situ* strain rate in the lower lithosphere assuming values of activation energies. Conversely, if the strain rate is known (for instance, from subduction velocity data) it is possible to evaluate activation energies using lithospheric age data. Determination of joint influence of strain rate and activation energies on flexure of the young lithosphere requires precise knowledge of its age.

COMPARISON WITH DATA

Using developed theory we analysed data across the Kuril trench where the subducting lithosphere presents age about the border between the Upper and the Lower Cretaceous, i.e. 100 Ma ranging between 90 Ma and 110 Ma (Nikolayev 1988) that is nearly constant along the trench. In addition, this area does not contain too many seamounts, ridges or fracture zones so that the analysis can be made using a large set of unperturbed profiles. Moreover, the trench is straight and long, whilst both changes in the trench direction and trench junctions disturb the outer rise geometry (Deplus & Dubois 1989). Finally we note that an estimate of strain rate, averaged over the lithospheric thickness, was given for the Kuril trench by McNutt & Menard (1982) using a quite different approach. Thus the Kuril trench appears to be a good test for our model.

The model may be applied to interpret both gravity and bathymetry data. As it was already discussed (e.g. Watts & Talwani 1974) results obtained using gravity profiles are more reliable, since shipboard marine gravity data naturally filter the short-wavelength noise that can be present in bathymetry. Furthermore, and more importantly, the gravity profiles are less affected by the sedimentary cover. The presence of sediments can result in a bathymetry that does not represent the flexure of the lithosphere. In addition, flexure is also visible in satellite altimetry (McAdoo & Martin 1984) so that abundant satellite altimeter data allow us to make a complete regional analysis by the same method.

In the present study, we used gravity profiles supplied by

the Bureau Gravimétrique International. 12 orthodromic profiles, 800 km long, were constructed by interpolation from all randomly distributed data points available in the area. The profiles were taken perpendicular to the trench (Fig. 13). The spacing along each profile is 7 km. Note that special care was taken to accomplish interpolations only in areas with sufficiently dense coverage of data and to avoid

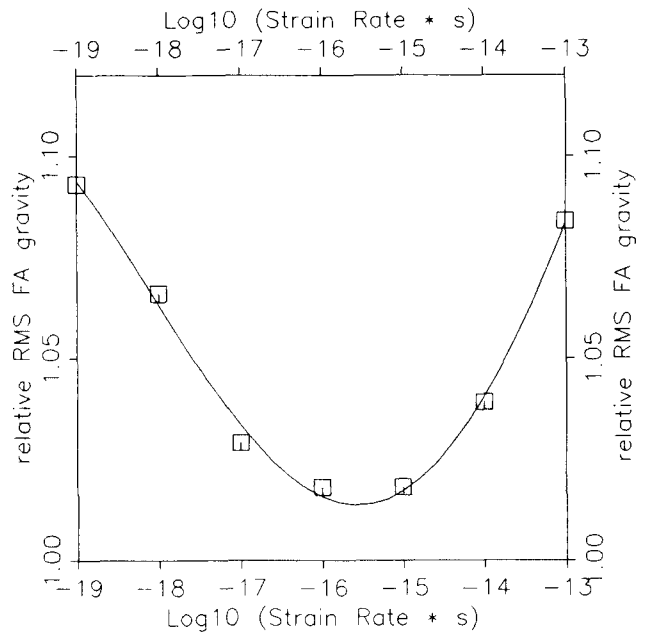


Figure 14. Averaged relative rms misfits between gravity data and model profiles. Since free-air gravity anomaly rms deviations between data and model profiles have a marked range difference because of diverse roughness of data profiles, we normalized rms misfits for each profile to the respective minimal value. Then relative rms misfits have been averaged through all the profiles. A pronounced minimal rms misfit (vertical axis) at the strain rate $\{\dot{\epsilon}: \log_{10}[\dot{\epsilon}(s^{-1}) \cdot s], \text{ horizontal axis}\}$ of about $3.10 \cdot 10^{16} s^{-1}$ is observed.

the junctions with Aleutian and Japanese trenches as well as seamounts, ridges and fracture zones.

The modelling of profiles was achieved assuming an age of 100 Ma and varying the strain rate that can represent, as it was shown above, variations of activation energies. The estimated strain rate lies between 10^{-16} s^{-1} and 10^{-15} s^{-1} assuming usual $Q_1 = 536 \text{ kJ/mole}$ and $Q_2 = 523 \text{ kJ/mole}$ (Fig. 14). On the basis of a relationship between strain rate in the oceanic lithosphere, outer-rise geometry and subduction rate derived from the purely elastic model, McNutt & Menard (1982) evaluated strain rate for several trenches; in particular, for the Kuril trench $\dot{\epsilon} = 1.4 \cdot 10^{-16} \text{ s}^{-1}$ that is consistent with our results. Hence the values of activation energies used seem to be reasonable. Note that our model does not use any information about subduction rate. Taking into account the lithospheric age range mentioned above as well as uncertainty of strain rate, according to Figs 3(a) and 7–11, we obtain on the whole trench approximately: $T_m = z_b = 61 \pm 3 \text{ km}$, $|w_B| = 435 \pm 30 \text{ m}$, $x_B = 86 \pm 4 \text{ km}$, $\Delta g_B = 38 \pm 3 \text{ mGal}$, $|x_H| = 75 \pm 4 \text{ km}$, $|z_H| = 45 \pm 3 \text{ km}$. Finally, from Table 1, temperature at depth z_b is about $750 \pm 20^\circ \text{C}$.

CONCLUSIONS

We developed a model of flexure of the oceanic lithosphere assuming a realistic rheology in order to estimate the strain rate of the lower oceanic lithosphere.

The mechanical lithosphere thickness appears to be controlled not only by the age, i.e. by the temperature distribution, but also by the strain rate and creep activation energy in the lower lithosphere. We computed flexure of the oceanic lithosphere at subduction zones for lithospheric ages ranging from 30 Ma to 160 Ma and strain rates from 10^{-19} s^{-1} up to 10^{-13} s^{-1} at activation energies $Q_1 = 536 \text{ kJ/mole}$ and $Q_2 = 523 \text{ kJ/mole}$. Analysis of the trade-offs among thermal structure represented as lithospheric age, activation energies, and strain rates allows us to extend the results of our modelling to consider different activation energy values.

Tests of the model show that from observations of flexure it is possible to estimate either the *in situ* strain rate or the *in situ* activation energies or the lithospheric age if other of these parameters are known. The accuracy of such estimation is better for old lithosphere. For young lithosphere (70 Ma or less), a precise knowledge of age is crucial. Use of independent estimations of strain rate, activation energies, and age based on different approaches improves the accuracy of rheology parameter evaluations. In this case a best-fit set of rheology parameters can be obtained.

ACKNOWLEDGMENTS

We are indebted to G. Balmino for the supply of gravity data and computer time. We thank G. Balma and M. Sarrailh as well as A. Cazenave and K. Dominh for providing sea gravity and some Geosat altimeter data. We thank M. G. Kogan for numerous helpful discussions. We appreciated the comments of two anonymous reviewers.

REFERENCES

- Bodine, J. H., Steckler, M. S. & Watts, A. B., 1981. Observations of flexure and the rheology of the oceanic lithosphere, *J. geophys. Res.*, **86**, 3695–3707.
- Bodine, J. H. & Watts, A. B., 1979. Lithospheric flexure seaward of the Bonin and Mariana trenches, *Earth planet. Sci. Lett.*, **43**, 132–148.
- Brace, W. F. & Kohlstedt, D. L., 1980. Limits on lithospheric stress imposed by laboratory experiments, *J. geophys. Res.*, **85**, 6248–6252.
- Byerlee, J., 1978. Friction of rocks, *Pure & appl. Geophys.*, **116**, 615–626.
- Caldwell, J. G., Haxby, W. F., Karig, D. E. & Turcotte, D. L., 1976. On the applicability of a universal elastic trench profile, *Earth planet. Sci. Lett.*, **31**, 239–246.
- Cazenave, A., 1984. Two distinct trends for cooling of the oceanic lithosphere, *Nature*, **310**, 401–403.
- Chamot-Rooke, N. & Le Pichon, X., 1989. Zenuis Ridge: mechanical model of formation, *Tectonophysics*, **160**, 175–193.
- Chapple, W. M. & Forsyth, D. W., 1979. Earthquakes and bending of plates at trenches, *J. geophys. Res.*, **84**, 6729–6749.
- De Bremaecker, J. C., 1977. Is the oceanic lithosphere elastic or viscous, *J. geophys. Res.*, **82**, 2001–2004.
- Denlinger, R. P., 1992. A revised estimate for the temperature structure of the oceanic lithosphere, *J. geophys. Res.*, **97**, 7219–7222.
- Deplus, Ch., 1987. Comportement mécanique de la lithosphère océanique, cas d'une subduction complexe, *PhD thesis*. Université Paris-Sud.
- Deplus, Ch. & Dubois, J., 1989. Flexural response of the oceanic lithosphere at an arc–arc junction: implication for the subduction of aseismic ridges, *Tectonophysics*, **160**, 63–73.
- Fadaie, K. & Ranalli, G., 1990. Rheology of the lithosphere in the East African rift system, *Geophys. J. Int.*, **102**, 445–453.
- Goetze, C. & Evans, B., 1979. Stress and temperature in the bending lithosphere as constrained by experimental rock mechanics, *Geophys. J. R. astr. Soc.*, **59**, 463–478.
- Gunn, R., 1943. A quantitative study of isobaric equilibrium and gravity anomalies in the Hawaiian islands, *J. Franklin. Inst.*, **236**, 373–390.
- Hanks, T. C., 1971. The Kuril Trench–Hokkaido Rise system: large shallow earthquakes and simple models of deformation, *Geophys. J. R. astr. Soc.*, **23**, 173–189.
- Ivanov, S. S., 1989. Stresses in an oceanic lithosphere associated with its curvature changes during its cooling, *Rep USSR Acad. Sci.*, **309**, 4, 838–841 (in Russian).
- Kirby, S. H., 1977. State of stress in the lithosphere: inferences from the flow laws of olivine, *Pure appl. Geophys.*, **115**, 245–258.
- Kirby, S. H., 1983. Rheology of the lithosphere, *Rev. Geophys. Space Phys.*, **21**, 1458–1487.
- Kirby, S. H. & Kronenberg, A. K., 1987. Rheology of the lithosphere: selected topics, *Rev. Geophys. Space Phys.*, **25**, 1219–1244.
- Lobkovsky, L. I. & Sorokhtin, O. G., 1976. Plastic deformations of the lithosphere at a subduction zone, in *Tectonics of Lithospheric Plates*, pp. 22–52, Ed. Sorokhtin, O. G., IOAN, Moscow (in Russian).
- McAdoo, D. C., Caldwell, J. G. & Turcotte, D. L., 1978. On the elastic–perfectly plastic bending of the lithosphere under generalized loading with application to the Kuril trench, *Geophys. J. R. astr. Soc.*, **54**, 11–26.
- McAdoo, D. C. & Martin, C. F., 1984. Seasat observations of lithospheric flexure seaward of trenches, *J. geophys. Res.*, **89**, 3201–3210.
- McAdoo, D. C., Martin, C. F. & Poulouse, S., 1985. Seasat observations of flexure: evidence for a strong lithosphere, *Tectonophysics*, **116**, 209–222.
- McNutt, M. K. & Menard, H. W., 1982. Constraints on yield

- strength in the oceanic lithosphere derived from observations of flexure, *Geophys. J. R. astr. Soc.*, **71**, 363–394.
- Melosh, H. J., 1978. Dynamic support of the outer rise, *Geophys. Res. Lett.*, **5**, 321–324.
- Nikolayev, N. I., 1988. *The Newest Tectonics and Geodynamics of the Lithosphere*, Nedra, Moscow (in Russian).
- Parker, R. L., 1972. The rapid calculation of potential anomalies, *Geophys. J. R. astr. Soc.*, **31**, 447–455.
- Parker, R. L. & Oldenburg, D. W., 1973. Thermal model of ocean ridges, *Nature*, **242**, 122, 137–139.
- Parsons, B. & Molnar, P., 1976. The origin of outer topographic rises associated with trenches, *Geophys. J. R. astr. Soc.*, **45**, 707–712.
- Parsons, B. & Sclater, J. G., 1977. An analysis of the variation of ocean floor bathymetry with age, *J. geophys. Res.*, **82**, 803–827.
- Ranalli, G. & Murphy, D. C., 1987. Rheological stratification of the lithosphere, *Tectonophysics*, **132**, 281–295.
- Stein, C. A. & Stein, S., 1992. A model for the global variation in oceanic depth and heat flow with lithospheric age, *Nature*, **359**, 123–129.
- Talwani, M., Worzel, J. L. & Landisman, M., 1959. Rapid gravity computations for two-dimensional bodies with applications to the Mendocino submarine fracture zone, *J. geophys. Res.*, **64**, 49–59.
- Turcotte, D. L., McAdoo, D. C. & Caldwell, J. G., 1978. An elastic-perfectly plastic analysis of the bending of the lithosphere at a trench, *Tectonophysics*, **47**, 193–205.
- Turcotte, D. L. & Oxburgh, E. R., 1967. Finite amplitude convective cells and continental drift, *J. Fluid Mech.*, **28**, 29–42.
- Turcotte, D. L. & Schubert, G., 1982. *Geodynamics applications of continuum physics to geological problems*, John Wiley & Sons, New York.
- Vening-Meinesz, F. A., 1941. Gravity over the Hawaiian Archipelago and over the Madeira Area: conclusions about the Earth's crust. *Proc. Kon. Ned. Akad. Wetensch.*, **44**, 1–12.
- Watts, A. B. & Talwani, M., 1974. Gravity anomalies seaward of deep-sea trenches and their tectonic implications, *Geophys. J. R. astr. Soc.*, **36**, 57–90.

APPENDIX A

The highest permissible difference of the principle stresses in the upper oceanic lithosphere (brittle layers)

We call normal, tangent and principle stresses as σ_n , σ_t and $\sigma_3 \leq \sigma_2 \leq \sigma_1$ respectively. For the plane area parallel to the direction of σ_2 and making an angle α between its normal and the direction of σ_1 , the Mohr's external circle relationship gives (e.g. Turcotte & Schubert 1982):

$$\sigma_n = \frac{\sigma_1 + \sigma_3}{2} + \frac{\sigma_1 - \sigma_3}{2} \cos 2\alpha; \quad \sigma_t = \frac{\sigma_1 - \sigma_3}{2} \sin 2\alpha. \quad (\text{A1})$$

Byerlee's laws [see eq. (1) above] can be represented in the general form as $\tau = A\sigma_n + B$. It means $\sigma_t = \tau$ if the difference of the principle stresses reaches its highest permissible value $\Delta\sigma_{\max} \equiv (\sigma_1 - \sigma_3)_{\max}$ at given σ_1 or σ_3 . Using (1) and (A1) it can be written as

$$(\sin 2\alpha - A - A \cos 2\alpha)\sigma_1 = (\sin 2\alpha + A - A \cos 2\alpha)\sigma_3 + 2B. \quad (\text{A2})$$

On the other hand, (A1) gives $\sigma_t^2 = -(\sigma_n - \sigma_3)(\sigma_n - \sigma_1)$. By differentiation at $\Delta\sigma_{\max}$ and taking into account $d\tau/d\sigma_n = A$, we find:

$$2A\tau = -(\sigma_n - \sigma_1) - (\sigma_n - \sigma_3) = \sigma_1 + \sigma_3 - 2\sigma_n. \quad (\text{A3})$$

A substitution of (A1) taken at $\Delta\sigma_{\max}$ for (A3) gives $A = -\text{ctg } 2\alpha$. Because $\sin 2\alpha \geq 0$, we have $\sin 2\alpha = (1 + A^2)^{-1/2}$ and $\cos 2\alpha = -A(1 + A^2)^{-1/2}$ so that (A2) can be rewritten as

$$[(1 + A^2)^{1/2} - A]\sigma_1 = [(1 + A^2)^{1/2} + A]\sigma_3 + 2B. \quad (\text{A4})$$

Let us consider the elastic stress that is supported by the plate until $\Delta\sigma_{\max}$ is reached. We assume that only lithostatic initial stress exists in the plate from its formation time. Generally the plate is deformed as long as it moves away from the mid-ocean ridge and even changes the sign of its curvature (Ivanov 1989), but stress must relax with time. In addition a specific cooling regime is observed for the oceanic lithosphere younger than 30 Ma (Cazenave 1984). Since we examine the plate older than 30 Ma, we shall not consider these features. We write for the non-deformed plate: $\sigma_{xx} = \sigma_{yy} = \sigma_{zz} = \sigma_1 = \sigma_2 = \sigma_3 = p$ where p is the lithostatic pressure. According to Hooke's law, we get

$$\begin{cases} E\varepsilon_{xx} = \sigma_{xx} - \nu\sigma_{yy} - \nu\sigma_{zz} = (1 - 2\nu)p \\ E\varepsilon_{yy} = -\nu\sigma_{xx} + \sigma_{yy} - \nu\sigma_{zz} = (1 - 2\nu)p. \\ E\varepsilon_{zz} = -\nu\sigma_{xx} - \nu\sigma_{yy} + \sigma_{zz} = (1 - 2\nu)p \end{cases} \quad (\text{A5})$$

If there is an additional stress $\Delta\sigma_{xx} \equiv \Delta\sigma$, but deformation remains in the x - z plane, i.e. $\Delta\varepsilon_{yy} = 0$, then the new stress and deformation are $\hat{\sigma}_{xx} = p + \Delta\sigma$, $\hat{\sigma}_{zz} = p$, and $\hat{\varepsilon}_{yy} = (1 - 2\nu)p/E$. Together with (A5), this results in

$$\begin{cases} E\hat{\varepsilon}_{xx} = p + \Delta\sigma - \nu\hat{\sigma}_{yy} - \nu p \\ (1 - 2\nu)p = -\nu(p + \Delta\sigma) + \hat{\sigma}_{yy} - \nu p \\ E\hat{\varepsilon}_{zz} = -\nu(p + \Delta\sigma) - \nu\hat{\sigma}_{yy} + p \end{cases}$$

hence

$$\begin{cases} \hat{\sigma}_{xx} - \sigma_{xx} = \Delta\sigma \\ \hat{\sigma}_{yy} - \sigma_{yy} = \nu\Delta\sigma. \\ \hat{\sigma}_{zz} - \sigma_{zz} = 0 \end{cases}$$

Poisson's ratio for rocks is restricted as $0.03 < \nu \leq 0.4$ (Turcotte & Schubert 1982). Therefore the principle stresses become

$$\begin{cases} \sigma_1 = \sigma_{xx} = p + \Delta\sigma \\ \sigma_2 = \sigma_{yy} = p + \nu\Delta\sigma \quad \text{if } \Delta\sigma > 0, \\ \sigma_3 = \sigma_{zz} = p \end{cases}$$

and

$$\begin{cases} \sigma_1 = \sigma_{zz} = p \\ \sigma_2 = \sigma_{yy} = p - \nu|\Delta\sigma| \quad \text{if } \Delta\sigma \leq 0. \\ \sigma_3 = \sigma_{xx} = p - |\Delta\sigma| \end{cases} \quad (\text{A6})$$

We note that the pressure has changed:

$$P = (\sigma_1 + \sigma_2 + \sigma_3)/3 = p + (1 + \nu)\Delta\sigma/3.$$

We define the signed $\Delta\sigma_{\max}$ that delimits the YSE as

$$\Delta\sigma_r = (\sigma_1 - \sigma_3)_{\max} \text{ sign}(P - p) \quad (\text{A7})$$

so that $\Delta\sigma_r > 0$ for compression and $\Delta\sigma_r < 0$ for tension. Substituting (A6) in (A4), we have

$$\Delta\sigma_r = 2(Ap + B) \begin{cases} [A + (1 + A^2)^{1/2}] \text{ for compression.} \\ [A - (1 + A^2)^{1/2}] \text{ for tension.} \end{cases} \quad (\text{A8})$$

Taking into account that $dp/dz = \rho g$, the following relation holds for each layer where A , B and ρ are constant:

$$\frac{d\Delta\sigma_r}{dz} \equiv \begin{cases} \gamma_{BC} \\ \gamma_{BT} \end{cases} = 2A\rho g \begin{cases} [A + (1 + A^2)^{1/2}] \text{ for compression.} \\ [A - (1 + A^2)^{1/2}] \text{ for tension.} \end{cases} \quad (\text{A9})$$

Note that actual values of A give $\gamma_{BC}/\gamma_{BT} \approx -(4 \pm 1)$.

At last we can determine the dependence of $\Delta\sigma_r$ on depth keeping in mind the continuity between (1a) and (1b) at $\sigma_n = 0.2$ GPa. The greatest Mohr's circle fitting both (1a) and (1b) may be derived from (A4). It corresponds to $\sigma_1 = 530$ MPa and $\sigma_3 = 113$ MPa with respective $\Delta\sigma_{\max} = 417$ MPa. Substituting in (A8) for A and B their values from (1), we find

$$\Delta\sigma_r = \begin{cases} 3.69p \text{ at } 0 \leq p \leq 113 \text{ MPa} \\ 2.12p + 177 \text{ MPa at } p > 113 \text{ MPa} \end{cases} \quad (\text{A10a})$$

for compression.

$$\Delta\sigma_r = \begin{cases} -0.787p \text{ at } 0 \leq p \leq 530 \text{ MPa} \\ -0.68p - 57 \text{ MPa at } p > 530 \text{ MPa} \end{cases} \quad (\text{A10b})$$

for tension.

Taking into account loading of the roughly 5 km deep ocean, we get

$$p(z) = 0.05 \text{ GPa} + g \begin{cases} \rho_c z \text{ at } 0 \leq z \leq T_c \\ \rho_c T_c + \rho_m(z - T_c) \text{ at } z > T_c \end{cases} \quad (\text{A11})$$

where z is the depth below the mean ocean-floor level, g is gravity acceleration, ρ_c is oceanic crust density, ρ_m is upper mantle density, T_c is oceanic crust thickness. Substituting $\rho_c \approx 2.8 \cdot 10^3 \text{ kg m}^{-3}$, $\rho_m \approx 3.3 \cdot 10^3 \text{ kg m}^{-3}$, $T_c \approx 6 \text{ km}$, $g \approx 9.8 \text{ m s}^{-2}$, we find $p = 113$ MPa at $z \approx 2.3 \text{ km}$ in the crust and $p = 530$ MPa at $z \approx 15.7 \text{ km}$ in the upper mantle. Thus shear stress in the tensional regime follows (1a) down to $z \approx 16 \text{ km}$, while for compression, shear stress is mainly (below $z \approx 2.3 \text{ km}$) represented by (1b). Finally substituting (A11) in (A10) we have

$$\Delta\sigma_r(z) = \begin{cases} 185 + 101z \text{ MPa at } 0 \leq z \leq 2.3 \text{ km} \\ 283 + 58z \text{ MPa at } 2.3 \leq z \leq 6 \text{ km} \\ 223 + 68z \text{ MPa at } z > 6 \text{ km} \end{cases} \quad (\text{A12a})$$

$$\Delta\sigma_r(z) = \begin{cases} -38 - 22z \text{ MPa at } 0 \leq z \leq 6 \text{ km} \\ -17 - 25.4z \text{ MPa at } 6 \leq z \leq 15.7 \text{ km} \\ -71 - 22z \text{ MPa at } z > 15.7 \text{ km} \end{cases} \quad (\text{A12b})$$

for compression and tension respectively (see Fig. 1).

APPENDIX B

Notation list

YSE—yield stress envelope;
 A , B —general coefficients of Byerlee's laws: $\tau = A\sigma_n + B$;
 a —thermal plate thickness;
 C —local constants in formulae;
 D —rigidity;
 E —Young's modulus;
 g —gravity acceleration;
 k —thermal diffusivity;
 M —the bending moment;
 OX —horizontal coordinate axis, perpendicular to the

trench, oceanward positive;
 OY —horizontal coordinate axis, parallel to the trench;
 OZ —vertical coordinate axis, downward positive;
 P —pressure;
 p —lithostatic pressure;
 Q —activation energy;
 R —gas constant;
 T —temperature;
 T_0 —zero-age temperature;
 T_c —oceanic-crust thickness;
 T_e —thickness of the elastic layer;
 T_m —thickness of the mechanical lithosphere;
 t —time (age);
 w —vertical deflection of the plate;
 w_B —outer-rise height (taken as a negative value);
 x_B —horizontal coordinate of the outer-rise crest;
 x_H —horizontal coordinate of the most intense flexure of the lithosphere;
 z —depth below the mean ocean-floor level;
 z_0 —neutral-plane depth below the mean ocean-floor level;
 z_B —depth (below the mean ocean-floor level) of the upper level of the elastic layer between elastic and brittle ones;
 z_D —depth (below the mean ocean-floor level) of the lower level of the elastic layer between elastic and ductile ones;
 z_n —depth (below the mean ocean-floor level) of the base of the mechanical lithosphere;
 z_H —domain depth (below sea-level) of the minimal thickness of the elastic layer;
 α —angle between the normal to the plane area and the direction of the greatest principle stress σ_1 ;
 γ_B , γ_D —either γ_{BC} and γ_{DT} , or γ_{BT} and γ_{DC} ;
 γ_{BC} —vertical gradient of $\Delta\sigma_r$ at compression in brittle layers;
 γ_{BT} —vertical gradient of $\Delta\sigma_r$ at tension in brittle layers;
 γ_L —absolute value of the vertical gradient of $\Delta\sigma_r$ in lower ductile layers: $\gamma_L = |\gamma_{DT}| = |\gamma_{DC}|$;
 γ_{DC} —vertical gradient of $\Delta\sigma_r$ at compression in ductile layers;
 γ_{DT} —vertical gradient of $\Delta\sigma_r$ at tension in ductile layers;
 Δg_B —maximal, free-air gravity anomaly over the outer rise;
 $\Delta\sigma$ —additional stress, compressive positive;
 $\Delta\sigma_{\max}$ —highest permissible difference of the principle stresses: $\Delta\sigma_{\max} \equiv (\sigma_1 - \sigma_3)_{\max}$;
 $\Delta\sigma_r$ —signed highest permissible (restrictive) difference of the principle stresses: $\Delta\sigma_r = \Delta\sigma_{\max} \text{ sign}(P - p)$;
 ε —deformations (with respective indices);
 $\dot{\varepsilon}$ —strain rate;
 λ —flexural parameter;
 ν —Poisson's ratio;
 ρ —density;
 ρ_c —oceanic-crust density;
 ρ_m —upper mantle density;
 ρ_w —sea-water density;
 σ_0 —a local constant in the creep law (2a);
 $\sigma_3 \leq \sigma_2 \leq \sigma_1$ —the principle stresses, compressive positive;
 σ_n —normal (confining) stress, compressive positive;
 σ_t —tangent (breaking) stress, compressive positive;
 σ_{xx} —normal stress along the OX -axis, compressive positive;
 σ_{yy} —normal stress along the OY -axis, compressive positive;
 σ_{zz} —normal stress along the OZ -axis, compressive positive;
 τ —highest permissible tangent (shear breaking) stress.